Computational and Structural Biotechnology Journal 17 (2019) 1075–1081

COMPUTATIONAL AND STRUCTURAL BIOTECHNOLOGY JOURNAL

journal homepage: www.elsevier.com/locate/csbj

Mini Review

Directional Switching Mechanism of the Bacterial Flagellar Motor

Tohru Minamino [a,*], Miki Kinoshita [a], Keiichi Namba [a,b]

[a] Graduate School of Frontier Biosciences, Osaka University, 1-3 Yamadoaka, Suita, Osaka 565-0871, Japan
[b] RIKEN Center for Biosystems Dynamic Research & Spring-8 Center, 1-3 Yamadaoka, Suita, Osaka 565-0871, Japan

ARTICLE INFO

Article history:
Received 31 May 2019
Received in revised form 26 July 2019
Accepted 27 July 2019
Available online 31 July 2019

Keywords:
Adaptive remodeling
Bacterial flagellar motor
Chemotaxis
Cooperativity
Directional switching
Motility

ABSTRACT

Bacteria sense temporal changes in extracellular stimuli via sensory signal transducers and move by rotating flagella towards into a favorable environment for their survival. Each flagellum is a supramolecular motility machine consisting of a bi-directional rotary motor, a universal joint and a helical propeller. The signal transducers transmit environmental signals to the flagellar motor through a cytoplasmic chemotactic signaling pathway. The flagellar motor is composed of a rotor and multiple stator units, each of which acts as a transmembrane proton channel to conduct protons and exert force on the rotor. FliG, FliM and FliN form the C ring on the cytoplasmic face of the basal body MS ring made of the transmembrane protein FliF and act as the rotor. The C ring also serves as a switching device that enables the motor to spin in both counterclockwise (CCW) and clockwise (CW) directions. The phosphorylated form of the chemotactic signaling protein CheY binds to FliM and FliN to induce conformational changes of the C ring responsible for switching the direction of flagellar motor rotation from CCW to CW. In this mini-review, we will describe current understanding of the switching mechanism of the bacterial flagellar motor.

Contents

1. Introduction . . . 1075
2. Structure of the C Ring . . . 1076
 2.1. FliG . . . 1077
 2.2. FliM . . . 1077
 2.3. FliN . . . 1077
 2.4. Subunit Organization in the C Ring Structure . . . 1078
3. Structural Basis for the Rotational Switching Mechanism . . . 1078
4. Adaptive remodeling of the C ring . . . 1079
5. Summary and Perspectives . . . 1079
Acknowledgements . . . 1080
References . . . 1080

1. Introduction

Many bacteria possess flagella to swim in liquid media and move on solid surfaces. *Escherichia coli* and *Salmonella enterica* serovar Typhimurium (hereafter referred to *Salmonella*) are model organisms that have provided deep insights into the structure and function of the bacterial flagellum. The flagellum is composed of basal body rings and an axial structure consisting of at least three parts: the rod as a drive shaft, the hook as a universal joint and the filament as a helical propeller (Fig. 1A). The flagellar motor of *E. coli* and *Salmonella* consists of a rotor and a dozen stator units and is powered by an electrochemical potential of protons across the cytoplasmic membrane, namely proton motive force. Marine *Vibrio* and extremely alkalophilic *Bacillus* utilize sodium motive force as the energy source to drive flagellar motor rotation. The rotor is composed of the MS ring made of the transmembrane protein FliF and the C ring consisting of three cytoplasmic proteins, FliG, FliM and FliN. Each stator unit is composed of two transmembrane proteins, MotA and MotB, and acts as a transmembrane proton channel to

* Corresponding author.
E-mail address: tohru@fbs.osaka-u.ac.jp (T. Minamino).

https://doi.org/10.1016/j.csbj.2019.07.020

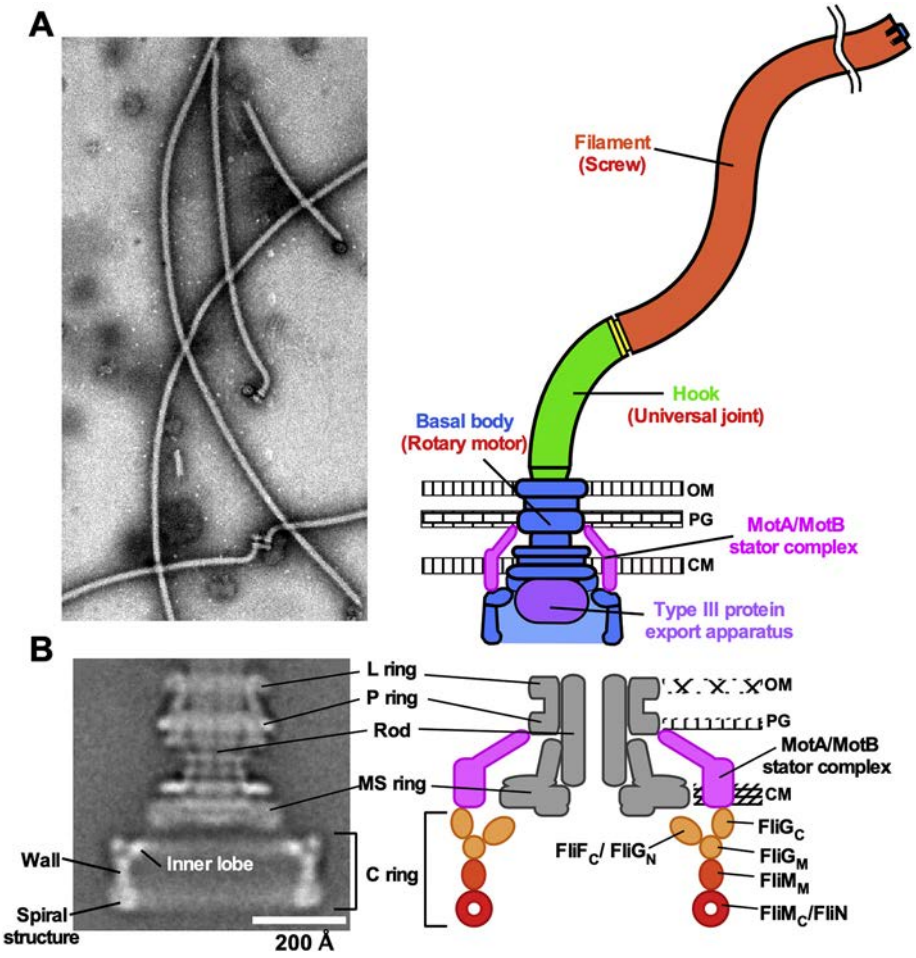

Fig. 1. Subunit organization in the flagellar motor. (A) Bacterial flagella. Electron micrograph of flagella purified from *Salmonella* on the left and its schematic diagram on the right. The flagellum is composed of the bsal body as a rotary motor, the hook as a universal joint and the filament as a molecular screw. (B) CryoEM image of *Salmonella* basal body on the left and its schematic diagram on the right. The purified basal body consists of the C, MS, L and P rings and the rod. A dozen MotA/MotB stator complexes are associated with the basal body but are lost during purification. The C ring is composed of FliG, FliM and FliN. The N-terminal domain of FliG ($FliG_N$) forms the inner lobe along with the C-terminal cytoplasmic domain of FliF ($FliF_C$). The C-terminal domain of FliG ($FliG_C$) is located in the upper part of the C ring wall. The middle domain of FliM ($FliM_M$) is located between the middle domain of FliG ($FliG_M$) and FliN and forms a cylindrical wall of the C ring. A continuous spiral density at the bottom edge of the C ring is made of the C-terminal domains of FliM ($FliM_C$) and FliN.

couple the proton flow through the channel with torque generation (Fig. 1B) [1–5].

The flagellar motor rotates in either counterclockwise (CCW; viewed from the flagellar filament to the motor) or clockwise (CW) direction in *E. coli* and *Salmonella*. When all the motors rotate in the CCW direction, flagellar filaments together form a bundle behind the cell body to push the cell forward. Brief CW rotation of one or more flagellar motors disrupts the flagellar bundle, allowing the cell to tumble, followed by a change in the swimming direction. Sensory signal transducers sense temporal changes in extracellular stimuli such as chemicals, temperature and pH and transmit such extracellular signals to the flagellar motor via the intracellular chemotactic signaling network. The phosphorylated form of CheY (CheY-P), which serves as a signaling molecule, binds to FliM and FliN in the C ring to switch the direction of flagellar motor rotation from CCW to CW. Thus, the C ring acts as a switching device to switch between the CCW and CW states of the motor [2,5].

The stator complex is composed of four copies of MotA and two copies of MotB. The $MotA_4/MotB_2$ complex is anchored to the peptidoglycan (PG) layer through direct interactions of the C-terminal periplasmic domain of MotB with the PG layer to become an active stator unit around the rotor [4]. A highly conserved aspartate residue of MotB (Asp-32 in the *E. coli* protein and Asp-33 in the *Salmonella* protein) is located in the $MotA_4/MotB_2$ proton channel and is involved in the energy coupling mechanism [6,7]. The cytoplasmic loop between transmembrane helices 2 and 3 of MotA ($MotA_C$) contains highly conserved Arg-90 and Glu-98 residues and are important not only for torque generation but also for stator assembly around the rotor [8–10].

FliG is directly involved in torque generation [8]. Highly conserved Arg-281 and Asp-289 residues are located on the torque helix of FliG ($Helix_{Torque}$) [11] and interact with Glu-98 and Arg-90 of $MotA_C$, respectively [8,10]. Since the elementary process of torque generation caused by sequential stator–rotor interactions in the flagellar motor is symmetric in the CCW and CW rotation, $Helix_{Torque}$ is postulated to rotate 180° relative to $MotA_C$ in a highly cooperative manner when the motor switches between the CCW and CW states of the C ring [12]. This mini-review article covers current understanding of how such a cooperative remodeling of the C ring structure occurs.

2. Structure of the C Ring

FliF assembles into the MS ring within the cytoplasmic membrane [13]. The C ring consisting of a cylindrical wall and inner lobes is formed by FliG, FliM and FliN on the cytoplasmic face of the MS ring with the inner lobes connected to the MS ring (Fig. 1B) [14]. FliF requires FliG to facilitate MS ring formation in the cytoplasmic membrane [15]. FliG binds to FliF with a one-to-one stoichiometry [16]. FliM and FliN together form the $FliM_1/FliN_3$ complex consisting of one copy of FliM and three copies of FliN [17], and the $FliM_1/FliN_3$ complex binds to the

FliG ring structure through a one-to-one interaction between FliG and FliM to form the continuous C ring wall [18–20]. Most of the domain structures of FliG, FliM and FliN have been solved at atomic resolution (Fig. 2), and possible models of their organization in the C ring have been proposed (Fig. 1B) [21,22].

2.1. FliG

FliG consists of three domains: N-terminal ($FliG_N$), middle ($FliG_M$) and C-terminal ($FliG_C$) domains (Fig. 2A) [23]. $FliG_C$ is divided into two subdomains: $FliG_{CN}$ and $FliG_{CC}$. $FliG_N$ is involved in the interaction with the C-terminal cytoplasmic domain of FliF ($FliF_C$) (Fig. 2B) [24,25]. Inter-molecular interactions between $FliG_N$ and $FliG_N$ and between $FliG_M$ and $FliG_{CN}$ are responsible for the assembly of FliG into the ring structure on the cytoplasmic face of the MS ring [26–29]. $FliG_M$ provides binding sites for FliM (Fig. 2C) [18–20]. A highly conserved EHPQR motif of $FliG_M$ is involved in the interaction with FliM [18,30]. $FliG_{CC}$ contains $Helix_{Torque}$, and highly conserved Arg-284 and Asp-292 residues of *Aquifex aeolicus* FliG, which corresponds to Arg-281 and Asp-289 of *E. coli* FliG involved in the interactions with conserved charged residues of $MotA_C$ [8,11], are exposed to solvent on the surface of $Helix_{Torque}$ [23].

2.2. FliM

FliM consists of three domains: N-terminal ($FliM_N$), middle ($FliM_M$) and C-terminal ($FliM_C$) domains [31,32]. $FliM_N$ contains a well conserved LSQXEIDALL sequence, which is responsible for the interaction with CheY-P [33]. $FliM_N$ is intrinsically disordered, and the binding of CheY-P to $FliM_N$ allows $FliM_N$ to become structured [32]. $FliM_M$ has a compactly folded conformation (Fig. 2C), and side-by-side associations between $FliM_M$ domains are responsible for the formation of the C ring wall [32]. The binding of CheY-P to $FliM_N$ affects inter-molecular $FliM_M$–$FliM_M$ interactions, thereby inducing a conformational change in the C ring responsible for switching the direction of flagellar motor rotation [34]. A well conserved GGXG motif of $FliM_M$ is involved in the interaction with $FliG_M$ (Fig. 2C) [18,30]. $FliM_C$ shows significant sequence and structural similarities with FliN and is responsible for the interaction with FliN (Fig. 2D) [35].

2.3. FliN

FliN is composed of an intrinsically disordered N-terminal region ($FliN_N$) and a compactly folded domain ($FliN_C$), which structurally looks similar to $FliM_C$ [36]. FliN exists as a dimer of dimer in solution (Fig. 2E) [37] and forms the $FliM_1/FliN_3$ complex along with FliM through an interaction between $FliM_C$ and FliN [17]. CheY-P binds to $FliN_C$ in a FliM-dependent manner [38]. Leu-68, Ala-93, Val-113 and Asp-116 of *E. coli* FliN are responsible for the interaction with CheY-P (Fig. 2D) [38,39]. The binding of CheY-P to FliN affects interactions between $FliM_C$ and FliN, inducing the conformational change of the C ring responsible for directional switching of flagellar motor rotation [38]. $FliN_N$ seems to control the binding affinity of $FliN_C$ for CheY-P [38] although it is dispensable for the function of FliN [40]. FliN also provides binding sites for FliH, a cytoplasmic component of the flagellar type III protein export apparatus for efficient flagellar protein export and assembly

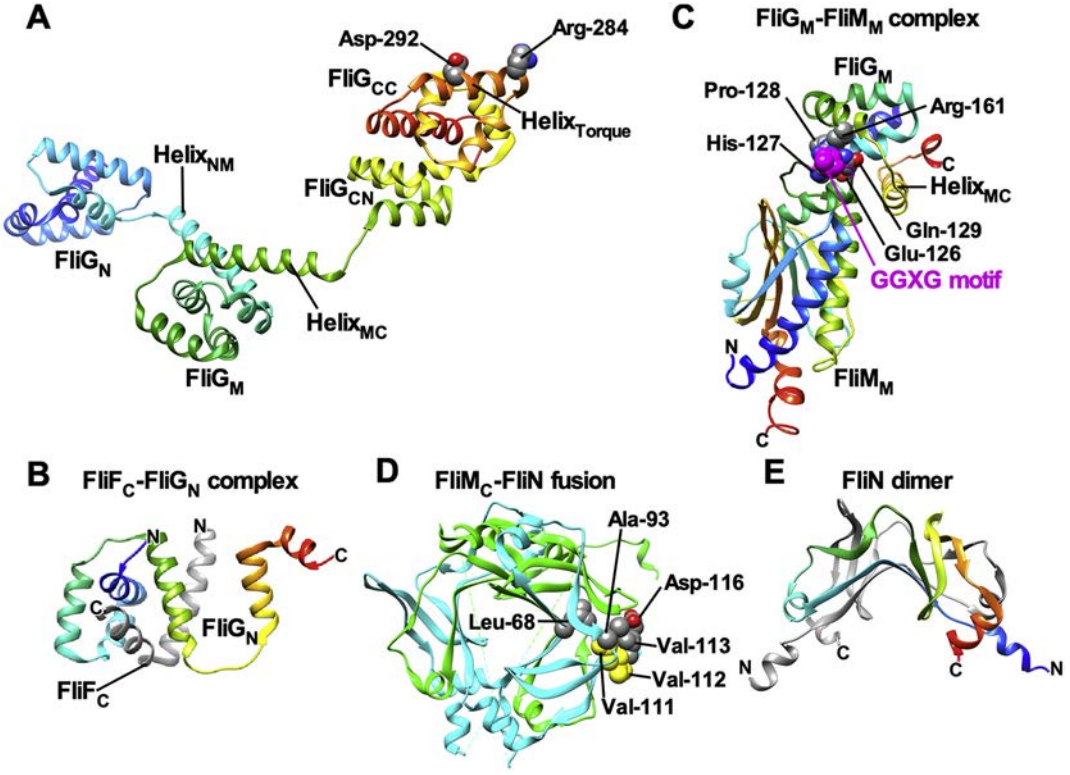

Fig. 2. Crystal structures of C ring proteins. (A) Crystal structure of FliG derived from *Aquifex aeolicus* (PDB code: 3HJL). The Cα backbone is colour-coded from blue to red, going through the rainbow colors from the N- to the C-terminus. FliG consists of $FliG_N$, $FliG_M$ and $FliG_C$ domains and two helix linkers, $Helix_{NM}$ and $Helix_{MC}$. $FliG_C$ is divided into $FliG_{CN}$ and $FliG_{CC}$ subdomains. Arg-284 and Asp-292 residues, which correspond to Arg-281 and Asp-289 of *E. coli* FliG, respectively, are located in the torque helix of $FliG_{CC}$ ($Helix_{Torque}$), which is involved in electrostatic interactions with the cytoplasmic loop of MotA. (B) Crystal structure of the $FliF_C/FliG_N$ complex derived from *Thermotaoga maritima* (PDB code: 5TDY). $FliF_C$ consisting of two α-helices (grey) binds to a hydrophobic groove of $FliG_N$ (rainbow). (C) Crystal structure of the $FliG_M/FliM_M$ complex derived from *T. maritima* (PDB code: 3SOH). A well conserved EHPQR motif in $FliG_M$ and a well conserved GGXG motif in $FliM_M$ are responsible for the $FliG_M$–$FliM_M$ interaction. (D) Crystal structure of *Salmonella* $FliM_C$–$FliN_N$ fusion protein (PDB code: 4YXB). $FliM_C$ and $FliN_N$ subunits are shown in green and cyan, respectively. Leu-68, Ala-93, Val-113 and Asp-116 of FliN are involved in the interaction with CheY-P. Val-111, Val-112 and Val-113 of FliN are required for the interaction with FliH. (E) Crystal structure of the FliN dimer derived from *T. maritima* (PDB code: 1YAB).

[36,39–42]. Val-111, Val-112 and Val-113 of FliN are responsible for the interaction with FliH (Fig. 2D) [39,41].

2.4. Subunit Organization in the C Ring Structure

Electron cryomicroscopy (cryoEM) image analysis has shown that the C ring structures of the purified CCW and CW motors have rotational symmetry varying from 32-fold to 35-fold, and the diameter varies accordingly [43,44]. The C ring diameters of the CCW and CW motors with C34 symmetry are 416 Å and 407 Å, respectively, and so the unit repeat distance along the circumference of the C ring is closer in the CW motor than in the CCW motor [45]. The C ring produced by a *Salmonella fliF–fliG* deletion fusion strain missing $FliF_C$ and $FliG_N$ lacks the inner lobe, suggesting that $FliF_C$ and $FliG_N$ together form the inner lobe (Fig. 1) [45,46]. In agreement with this, cryoEM images of the C ring containing the N-terminally green fluorescent protein (GFP) tagged FliG protein show an extra density corresponding to the GFP probe near the inner lobe [47]. The *fliF–fliG* deletion fusion results in unusual switching behavior of the flagellar motor, suggesting that the inner lobe is required for efficient and robust switching in the direction of flagellar motor rotation in response to changes in the environment [45]. The upper part of the C ring wall is formed by $FliG_M$ and $FliG_C$. $FliG_M$ binds to $FliG_{CN}$ of its adjacent FliG subunit to produce a domain-swap polymer of FliG to form a ring in both CCW and CW motors [26,27,29]. Since $Helix_{Torque}$ of $FliG_{CC}$ interacts with $MotA_C$ [8,10], $FliG_{CC}$ is located at the top of the C ring wall (Fig. 1). Since $FliM_M$ directly binds to $FliG_M$ (Fig. 2C) [18–20], the continuous wall of the C ring with a thickness of 4.0 nm and a height of 6.0 nm is formed by side-by-side associations of the $FliM_M$ domains (Fig. 1) [32]. A continuous spiral density with a diameter of 7.0 nm along the circumference at the bottom edge of the C ring is made of $FliM_C$ and FliN (Fig. 1) [17,36].

3. Structural Basis for the Rotational Switching Mechanism

In *E. coli* and *Salmonella*, the flagellar motor is placed in a default CCW state [3,5]. Mutations located in and around $Helix_{MC}$ of FliG, which connects $FliG_M$ and $FliG_{CN}$, cause unusual switching behavior of the flagellar motor [48], suggesting that $helix_{MC}$ is involved in switching the direction of flagellar motor rotation. $Helix_{MC}$ is located at the $FliG_M$–$FliM_M$ interface and contributes to hydrophobic interactions between $FliG_M$ and $FliM_M$ (Fig. 3A) [18,19]. In-frame deletion of three residues, Pro-Ala-Ala at positions 169 to 171 of *Salmonella* FliG, which are located in $Helix_{MC}$, locks the motor in the CW state even in the absence of CheY-P (CW-locked deletion) [49,50]. The crystal structure of the $FliG_M$ and $FliG_C$ domains derived from *Thermotaoga maritima* (Tm-$FliG_{MC}$) with this CW-locked deletion have shown that the conformation of $Helix_{MC}$ is distinct from that of the wild-type [19,50,51]. In the wild-type Tm-$FliG_{MC}$/Tm-$FliM_M$ complex, Val-172 of $Helix_{MC}$ of Tm-$FliG_{MC}$ makes hydrophobic contact with Ile-130 and Met-131 of Tm-$FliM_M$ (Fig. 3A) [18,19]. In contrast, disulfate crosslinking experiments have shown that $Helix_{MC}$ is dissociated from Tm-$FliG_M$ in the presence of the CW-locked deletion (Fig. 3A) [28]. Consistently, the CW-locked deletion of Tm-FliG reduces the binding affinity of Tm-$FliG_{MC}$ for Tm-$FliM_M$ by about 400-fold [28]. Therefore, it seems likely that the binding of CheY-P to FliM and FliN induces conformational rearrangements of the $FliG_M$–$FliM_M$ interface, thereby causing dissociation of $Helix_{MC}$ from the interface to facilitate the remodeling of the FliG ring structure responsible for directional switching of the flagellar motor.

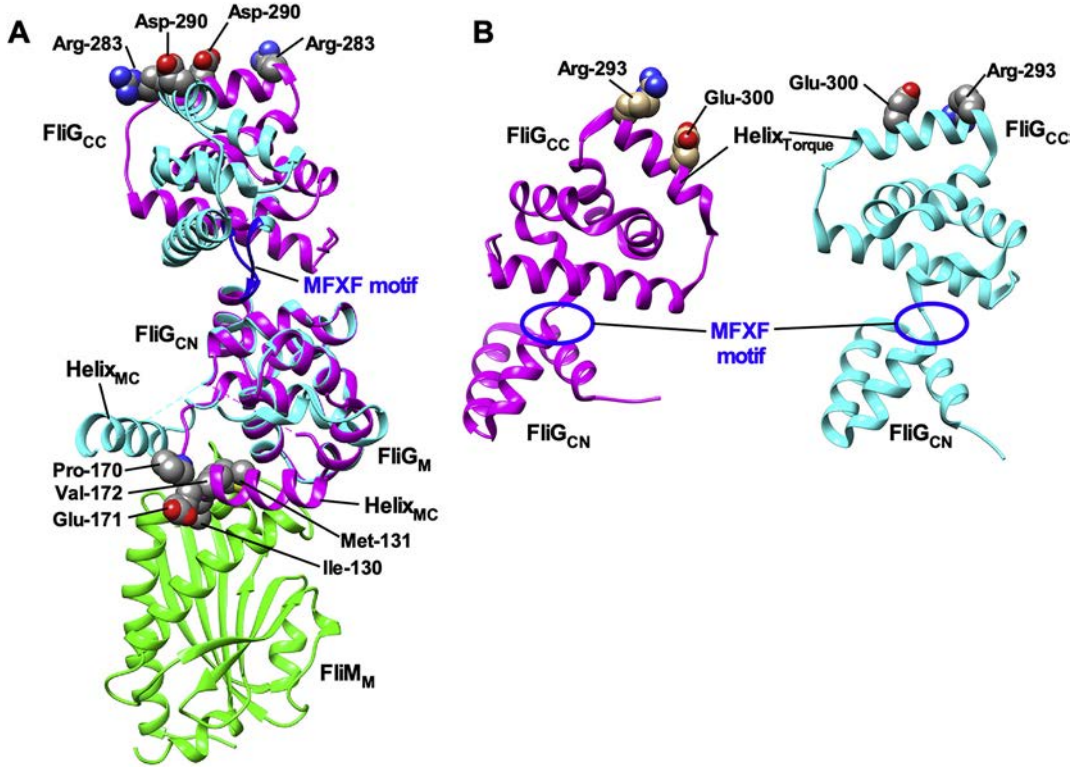

Fig. 3. Structural basis for the switching mechanism. (A) Structural comparisons between wild-type $FliG_M$ and $FliG_C$ domains of *T. maritima* (Tm-$FliG_{MC}$) and its CW-locked deletion variant, Tm-$FliG_{MC}$(ΔPEV). Cα ribbon drawing of Tm-$FliG_{MC}$ (magenta), Tm-$FliG_{MC}$(ΔPEV) (cyan) and Tm-$FliM_M$ (green). The $FliG_M$ domain of Tm-$FliG_{MC}$(ΔPEV) (PDB ID: 3AJC) was superimposed onto that of the Tm-$FliG_{MC}$/Tm-$FliM_M$ complex (PDB ID: 4FHR). $Helix_{MC}$ is located at an interface between $FliG_M$ and $FliM_M$. In contrast, the CW-locked deletion not only induces a distinct orientation of $Helix_{MC}$ relative to the $FliG_M$–$FliM_M$ interface but also goes through a 90° rotation of $FliG_{CC}$ through a conserved MFXF motif colored in blue. Arg-283 and Asp-290 of Tm-FliG correspond to Arg-281 and Asp-289 of *E. coli* FliG, respectively. (B) Comparisons between the 3USY (cyan) and 3USW (magenta) structures of *Helicobacter pylori* FliG. Conformational rearrangements of the conserved MFXF motif induces a 180° rotation of $FliG_{CC}$ relative to $FliG_{CN}$ to reorient Arg-293 and Glu-300 residues, which correspond to Arg-281 and Asp-289 of *E. coli* FliG, respectively.

$Helix_{MC}$ interacts with $Helix_{NM}$ connecting $FliG_N$ and $FliG_M$ (Fig. 2A) [23]. The E95D, D96V/Y, T103S, G106A/C and E108K substitutions in $Helix_{NM}$ of *Salmonella* FliG result in a strong CW switch bias [52]. A homology model of *Salmonella* FliG built based on the crystal structure of FliG derived from *A. aeolicus* (PDB code: 3HJL) has suggested that Thr-103 of $Helix_{NM}$ may make hydrophobic contacts with Pro-169 and Ala-173 of $Helix_{MC}$ [45]. These observations lead to a plausible hypothesis that a change in the $Helix_{NM}$–$Helix_{MC}$ interaction mode may be required for conformational rearrangements of the C ring responsible for directional switching of the flagellar motor. A FliF–FliG full length fusion results in a strong CW switch bias of the *E. coli* flagellar motor [27]. Intragenic suppressor mutations, which improve the chemotactic behavior of the *E. coli fliF–fliG* full-length fusion strain, are located at the $FliG_N$–$FliG_N$ interface [27], suggesting that a change in inter-molecular $FliG_N$–$FliG_N$ interactions may be required for flagellar motor switching. Therefore, there is the possibility that conformational rearrangements of the $FliG_M$–$FliM_M$ interface caused by the binding of CheY-P to the C ring influence the $Helix_{NM}$–$Helix_{MC}$ interaction, thereby inducing conformational rearrangements of $FliG_N$ domains responsible for the switching in the direction of flagellar motor rotation.

The elementary process of torque generation by stator-rotor interactions is symmetric in CCW and CW rotation [12]. A hinge connecting $FliG_{CN}$ and $FliG_{CC}$ has a highly flexible nature at the conserved MFXF motif, allowing $FliG_{CC}$ to rotate 180° relative to $FliG_{CN}$ to reorient Arg-281 and Asp-289 residues in $Helix_{Torque}$ to achieve a symmetric elementary process of torque generation in both CCW and CW rotation (Fig. 3B) [53–56]. Structural comparisons between Tm-$FliG_{MC}$ of the wild-type and Tm-$FliG_{MC}$ with the CW-locked deletion have shown that the CW-locked deletion induces a 90° rotation of $FliG_{CC}$ relative to $FliG_{CN}$ through the MFXF motif (Fig. 3A) [50]. Consistently, the binding of CheY-P to the C ring induces a tilting movement of $FliM_M$, resulting in the rotation of $FliG_{CC}$ relative to $FliG_{CN}$ [34]. Therefore, it is possible that such a tilting movement of $FliM_M$ may promote a detachment of $Helix_{MC}$ from the $FliG_M$–$FliM_M$ interface, resulting in the 180° rotation of $FliG_{CC}$ relative to $FliG_{CN}$.

4. Adaptive remodeling of the C ring

FliM and FliN alternate their forms between localized and freely diffusing ones (Fig. 4), and the copy number of FliM and FliN in the CCW motor has been found to be about 1.3 times larger than that in the CW motor [57–60]. Consistently, fluorescence anisotropy techniques have shown that the CCW motor accommodate more $FliM_1/FliN_3$ complexes without changing the spacing between FliM subunits [61]. Such exchanges depend on the direction of flagellar rotation but not on the binding of CheY-P to the C ring per se [58]. The timescale of this adaptive switch remodeling of the C ring structure is much slower (~ 1 min) than that of the rotational switching between the CCW and CW states (less than millisecond). Such a structural remodeling of the C ring is important for fine-tuning the chemotactic response to temporal changes in the environments [62–65]. The CW-locked deletion of FliG considerably reduces the binding affinity of $FliG_M$ for $FliM_M$ presumably due to detachment of $Helix_{MC}$ from the $FliG_M$–$FliM_M$ interface (Fig. 3A) [28]. Because FliM binds to $Helix_{MC}$ of FliG in the *E. coli* CCW motor [27], the dissociation of $Helix_{MC}$ from the $FliG_M$–$FliM_M$ interface may promote the dissociation of several weakly bound $FliM_1/FliN_3$ complexes from the FliG ring when CheY-P binds to the C ring to switch from its CCW to CW states (Fig. 4).

5. Summary and Perspectives

Switching between the CW and CCW states of the flagellar motor is highly cooperative [66]. The cooperative switching mechanism can be explained by a conformational spread model, in which a switching event is mediated by conformational changes in a ring of subunits that spread from subunit to subunit via their interactions along the ring [67–69]. The binding of CheY-P to FliM and FliN affects subunit-subunit interactions between $FliM_M$ domains and between $FliM_C$ and FliN in the C ring to induce a 180° rotation of $FliG_{CC}$ relative to $MotA_C$, thereby allowing the motor to rotate in CW direction [34]. $Helix_{MC}$ of FliG located at an interface between $FliG_M$ and $FliM_M$ plays an important role in highly cooperative remodeling of the FliG ring structure [28]. However, it remains unknown how $Helix_{MC}$ coordinates cooperative rearrangements of FliG subunits with changes in the direction of flagellar motor rotation. The C ring of the CCW motor can accommodate more $FliM/FliN_3$ complexes without changing inter-subunit spacing, and directional switching of the motor induces several weakly bound $FliM/FliN_3$ complexes from the C ring [57–60]. Consistently, the CW-locked deletion weakens an interaction between $FliG_M$ and $FliM_M$ [28]. Because there is no difference in the rotational symmetry of the C ring between the purified CCW and CW motors [45], it remains unclear how several $FliM_1/FliN_3$ complexes weakly associate with the C ring when the motor spins in the CCW direction.

The elementary process of the torque-generation cycle is symmetrical in CCW and CW directions [12]. However, the output characteristics of the CW motor are distinct from those of the CCW motor. Torque produced by the CCW motor remains almost constant in a high-load, low-load regime of the torque-speed curve and decreases sharply to zero in a low-load, high-speed regime. In contrast, torque produced by the CW motor linearly decreases with increasing motor speed [70]. This suggests that directional switching of the flagellar motor may affect stator–rotor interactions in a load-dependent manner. However,

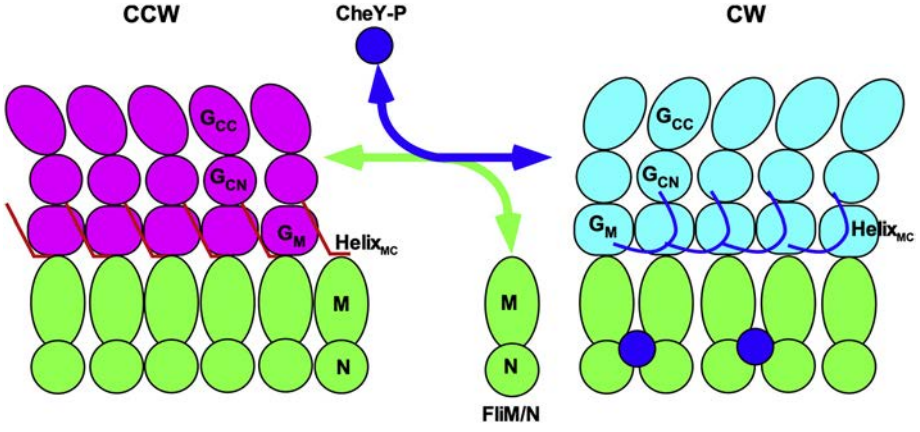

Fig. 4. Adaptive remodeling of the FliG ring in the CCW and CW motors. Inter-molecular interactions of $FliG_{CN}$ with $FliG_M$ of its neighboring subunit produce the CCW ring structure. Upon binding of CheY-P to the C ring, conformational rearrangements of the $FliG_M$–$FliG_C$ interface occur, resulting in detachment of $Helix_{MC}$ from the interface. As a result, several weakly bound $FliM_1/FliN_3$ complexes dissociate from the FliG ring.

nothing is known about the molecular mechanism. Furthermore, the switching rate of the flagellar motor also depends on the motor speed [71,72]. A recent non-equilibrium model of the flagellar motor switching has predicted that the motor sensitivity to CheY-P increases with an increase in motor torque [73]. However, it remains unknown how stator–rotor interactions modulate the binding affinity for CheY-P. High-resolution structural analysis of the C rings in the CCW and CW states by cryoEM image analysis will be essential to advance our mechanistic understanding of the directional switching mechanism of the flagellar motor.

Declaration of Competing Interest

The authors declare that they have no competing interests.

Acknowledgements

Our research is supported in part by the Japan Society for the Promotion of Science (JSPS KAKENHI Grant Numbers JP19H03182 to T.M., JP18K14638 to M.K. and JP25000013 to K.N.).

References

[1] Berg HC. The rotary motor of bacterial flagella. Annu Rev Biochem 2003;72:19–54.
[2] Morimoto YV, Minamino T. Structure and function of the bi-directional bacterial flagellar motor. Biomolecules 2014;4:217–34.
[3] Minamino T, Imada K. The bacterial flagellar motor and its structural diversity. Trends Microbiol 2015;23:267–74.
[4] Minamino T, Terahara N, Kojima S, Namba K. Autonomous control mechanism of stator assembly in the bacterial flagellar motor in response to changes in the environment. Mol Microbiol 2018;109:723–34.
[5] Nakamura S, Minamino T. Flagella-driven motility of bacteria. Biomoluecles 2019;9:279.
[6] Zhou J, Sharp LL, Tang HL, Lloyd SA, Billings S, et al. Function of protonatable residues in the flagellar motor of *Escherichia coli*: critical role for Asp 32 of MotB. J Bacteriol 1998;180:2729–35.
[7] Che YS, Nakamura S, Morimoto YV, Kami-ike N, Namba K, et al. Load-sensitive coupling of proton translocation and torque generation in the bacterial flagellar motor. Mol Microbiol 2014;91:175–84.
[8] Zhou J, Lloyd SA, Blair DF. Electrostatic interactions between rotor and stator in the bacterial flagellar motor. Proc Natl Acad Sci U S A 1998;95:6436–41.
[9] Morimoto YV, Nakamura S, Kami-ike N, Namba K, Minamino T. Charged residues in the cytoplasmic loop of MotA are required for stator assembly into the bacterial flagellar motor. Mol Microbiol 2010;78:1117–29.
[10] Morimoto YV, Nakamura S, Hiraoka KD, Namba K, Minamino T. Distinct roles of highly conserved charged residues at the MotA-FliG interface in bacterial flagellar motor rotation. J Bacteriol 2013;195:474–81.
[11] Lloyd SA, Whitby FG, Blair DF, Hill CP. Structure of the C-terminal domain of FliG, a component of the rotor in the bacterial flagellar motor. Nature 1999;400:472–5.
[12] Nakamura S, Kami-ike N, Yokota JP, Minamino T, Namba K. Evidence for symmetry in the elementary process of bidirectional torque generation by the bacterial flagellar motor. Proc Natl Acad Sci U S A 2010;107:17616–20.
[13] Ueno T, Oosawa K, Aizawa SI. M ring, S ring and proximal rod of the flagellar basal body of Salmonella typhimurium are composed of subunits of a single protein, FliF. J Mol Biol 1992;227:672–7.
[14] Francis NR, Sosinsky GE, Thomas D, DeRosier DJ. Isolation, characterization, and structure of bacterial flagellar motors containing the switch complex. J Mol Biol 1994;235:1261–70.
[15] Morimoto YV, Ito M, Hiraoka KD, Che YS, Bai F, Kami-Ike N, et al. Assembly and stoichiometry of FliF and FlhA in *Salmonella* flagellar basal body. Mol Microbiol 2014;91:1214–26.
[16] Levenson R, Zhou H, Dahlquist FW. Structural insights into the interaction between the bacterial flagellar motor proteins FliF and FliG. Biochemistry 2012;51:5052–60.
[17] McDowell MA, Marcoux J, McVicker G, Johnson S, Fong YH, et al. Characterisation of *Shigella* Spa33 and *Thermotoga* FliM/N reveals a new model for C-ring assembly in T3SS. Mol Microbiol 2016;99:749–66.
[18] Paul K, Gonzalez-Bonet G, Bilwes AM, Crane BR, Blair D. Architecture of the flagellar rotor. EMBO J 2011;30:2962–71.
[19] Vartanian AS, Paz A, Fortgang EA, Abramson J, Dahlquist FW. Structure of flagellar motor proteins in complex allows for insights into motor structure and switching. J Biol Chem 2012;287:35779–83.
[20] Lam KH, Lam WW, Wong JY, Chan LC, Kotaka M, Ling TK, et al. Structural basis of FliG-FliM interaction in *Helicobacter pylori*. Mol Microbiol 2013;88:798–812.
[21] Minamino T, Imada K, Namba K. Molecular motors of the bacterial flagella. Curr Opin Struct Biol 2008;18:693–701.
[22] Stock D, Namba K, Lee LK. Nanorotors and self-assembling macromolecular machines: the torque ring of the bacterial flagellar motor. Curr Opin Biotechnol 2012;23:545–54.
[23] Lee KL, Ginsburg MA, Crovace C, Donohoe M, Stock D. Structure of the torque ring of the flagellar motor and the molecular basis for rotational switching. Nature 2010;466:996–1000.
[24] Lynch MJ, Levenson R, Kim EA, Sircar R, Blair DF, Dahlquist FW, et al. Co-folding of a FliF-FliG split domain forms the basis of the MS:C ring interface within the bacterial flagellar motor. Structure 2017;25:317–28.
[25] Xue C, Lam KH, Zhang H, Sun K, Lee SH, et al. Crystal structure of the FliF-FliG complex from *Helicobacter pylori* yields insight into the assembly the motor MS–C ring in the bacterial flagellum. J Biol Chem 2018;293:2066–78.
[26] Baker MA, Hynson RM, Ganuelas LA, Mohammadi NS, Liew CW, Rey AA, et al. Domain-swap polymerization drives the self-assembly of the bacterial flagellar motor. Nat Struct Mol Biol 2016;23:197–203.
[27] Kim EA, Panushka J, Meyer T, Carlisle R, Baker S, Ide N, et al. Architecture of the flagellar switch complex of *Escherichia coli*: conformational plasticity of FliG and implications for adaptive remodeling. J Mol Biol 2017;429:1305–20.
[28] Kinoshita M, Furukawa Y, Uchiyama S, Imada K, Namba K, Minamino T. Insight into adaptive remodeling of the rotor ring complex of the bacterial flagellar motor. Biochem Biophys Res Commun 2018;496:12–7.
[29] Kinoshita M, Namba K, Minamino T. Effect of a clockwise-locked deletion in FliG on the FliG ring structure of the bacterial flagellar motor. Genes Cells 2018;23:241–7.
[30] Brown PN, Terrazas M, Paul K, Blair DF. Mutational analysis of the flagellar protein FliG: sites of interaction with FliM and implications for organization of the switch complex. J Bacteriol 2007;189:305–12.
[31] Mathews MA, Tang HL, Blair DF. Domain analysis of the FliM protein of *Escherichia coli*. J Bacteriol 1998;180:5580–90.
[32] Park SY, Lowder B, Bilwes AM, Blair DF, Crane BR. Structure of FliM provides insight into assembly of the switch complex in the bacterial flagella motor. Proc Natl Acad Sci U S A 2006;103:11886–91.
[33] Lee SY, Cho HS, Pelton JG, Yan D, Henderson RK, et al. Crystal structure of an activated response regulator bound to its target. Nat Struct Mol Biol 2001;8:52–6.
[34] Paul K, Brunstetter D, Titen S, Blair DF. A molecular mechanism of direction switching in the flagellar rotation of *Escherichia coli*. Proc Natl Acad Sci U S A 2011;108:17171–6.
[35] Sarkar MK, Paul K, Blair D. Subunit organization and reversal associated movements in the flagellar switch of *Escherichia coli*. J Biol Chem 2010;285:675–84.
[36] Notti RQ, Bhattacharya S, Lilic M, Stebbins CE. A common assembly module in injectisome and flagellar type III secretion sorting platforms. Nat Commun 2015;6:7125.
[37] Brown PN, Mathews MA, Joss LA, Hill CP, Blair DF. Crystal structure of the flagellar rotor protein FliN from *Thermotoga maritima*. J Bacteriol 2005;187:2890–902.
[38] Sarkar MK, Paul K, Blair D. Chemotaxis signaling protein CheY binds to the rotor protein FliN to control the direction of flagellar rotation in *Escherichia coli*. Proc Natl Acad Sci U S A 2010;107:9370–5.
[39] Paul K, Harmon JG, Blair DF. Mutational analysis of the flagellar rotor protein FliN: identification of surfaces important for flagellar assembly and switching. J Bacteriol 2006;188:5240–8.
[40] González-Pedrajo B, Minamino T, Kihara M, Namba K. Interactions between C ring proteins and export apparatus components: a possible mechanism for facilitating type III protein export. Mol Microbiol 2006;60:984–98.
[41] McMurry JL, Murphy JW, González-Pedrajo B. The FliN-FliH interaction mediates localization of flagellar export ATPase FliI to the C ring complex. Biochemistry 2006;45:11790–8.
[42] Minamino T, Yoshimura SDJ, Morimoto YV, González-Pedrajo B, Kami-ike N, et al. Roles of the extreme N-terminal region of FliH for efficient localization of the FliH-FliI complex to the bacterial flagellar type III export apparatus. Mol Microbiol 2009;74:1471–83.
[43] Thomas DR, Morgan DG, DeRosier DJ. Rotational symmetry of the C ring and a mechanism for the flagellar rotary motor. Proc Natl Acad Sci U S A 1999;96:10134–9.
[44] Thomas DR, Francis NR, Xu C, DeRosier DJ. The three-dimensional structure of the flagellar rotor from a clockwise-locked mutant of *Salmonella enterica* serovar Typhimurium. J Bacteriol 2006;188:7039–48.
[45] Sakai T, Miyata T, Terahara N, Mori K, Inoiue Y, et al. Novel insights into conformational rearrangements of the bacterial flagellar switch complex. mBio 2019;10 e00079–19.
[46] Thomas D, Morgan DG, DeRosier DJ. Structures of bacterial flagellar motors from two FliF-FliG gene fusion mutants. J Bacteriol 2001;183:6404–12.
[47] Morimoto YV, Kami-ike N, Miyata T, Kawamoto A, Kato T, et al. High-resolution pH imaging of living bacterial cell to detect local pH differences. mBio 2016;7:01911–6.
[48] Van Way SM, Millas SG, Lee AH, Manson MD. Rusty, jammed, and well-oiled hinges: mutations affecting the interdomain region of FliG, a rotor element of the *Escherichia coli* flagellar motor. J Bacteriol 2006;188:3944–51.
[49] Togashi F, Yamaguchi S, Kihara M, Aizawa SI, Macnab RM. An extreme clockwise switch bias mutation in *fliG* of *Salmonella typhimurium* and its suppression by slow-motile mutations in *motA* and *motB*. J Bacteriol 1997;179:2994–3003.
[50] Minamino T, Imada K, Kinoshita M, Nakamura S, Morimoto YV, Namba K. Structural insight into the rotational switching mechanism of the bacterial flagellar motor. PLoS Biol 2011;9:e1000616.
[51] Brown PN, Hill CP, Blair DF. Crystal structure of the middle and C-terminal domains of the flagellar rotor protein FliG. EMBO J 2002;21:3225–34.
[52] Irikura VM, Kihara M, Yamaguchi S, Sockett H, Macnab RM. *Salmonella typhimurium fliG* and *fliN* mutations causing defects in assembly, rotation, and switching of the flagellar motor. J Bacteriol 1993;175:802–10.

[53] Lam KH, Ip WS, Lam YW, Chan SO, Ling TK, Au SW. Multiple conformations of the FliG C-terminal domain provide insight into flagellar motor switching. Structure 2012;20:315–25.
[54] Pandini A, Morcos F, Khan S. The gearbox of the bacterial flagellar motor switch. Structure 2016;24:1209–20.
[55] Miyanoiri Y, Hijikata A, Nishino Y, Gohara M, Onoue Y, et al, Kojima M. Structural and functional analysis of the C-terminal region of FliG, an essential motor component of *Vibrio* Na^+-driven flagella. Structure 2017;25:1540–8.
[56] Nishikino T, Hijikata A, Miyanoiri Y, Onoue Y, Kojima S, Shirai T, et al. Rotational direction of flagellar motor from the conformation of FliG middle domain in marine *Vibrio*. Sci Rep 2018;8:17793.
[57] Delalez NJ, Wadhams GH, Rosser G, Xue Q, Brown MT, Dobbie IM, et al. Signal-dependent turnover of the bacterial flagellar switch protein FliM. Proc Natl Acad Sci U S A 2010;107:11347–51.
[58] Lele PP, Branch RW, Nathan VS, Berg HC. Mechanism for adaptive remodeling of the bacterial flagellar switch. Proc Natl Acad Sci U S A 2012;109:20018–22.
[59] Delalez NJ, Berry RM, Armitage JP. Stoichiometry and turnover of the bacterial flagellar switch protein FliN. mBio 2014;5:e01216–14.
[60] Branch RW, Sayegh MN, Shen C, Nathan VS, Berg HC. Adaptive remodeling by FliN in the bacterial rotary motor. J Mol Biol 2014;426:3314–24.
[61] Hosu BG, Berg HC. CW and CCW conformations of the E. coli flagellar motor C-ring evaluated by fluorescence anisotropy. Biophys J 2018;114:641–9.
[62] Yuan J, Branch RW, Hosu BG, Berg HC. Adaptation at the output of the chemotaxis signalling pathway. Nature 2012;484:233–6.
[63] Yuan J, Berg HC. Ultrasensitivity of an adaptive bacterial motor. J Mol Biol 2013;425:1760–4.
[64] Dufour YS, Fu X, Hernandez-Nunez L, Emonet T. Limits of feedback control in bacterial chemotaxis. PLoS Comput Biol 2014;10:e1003694.
[65] Lele PP, Shrivastava A, Roland T, Berg HC. Response thresholds in bacterial chemotaxis. Sci Adv 2015;1:e1500299.
[66] Cluzel P, Surette M, Leibler S. An ultrasensitive bacterial motor revealed by monitoring signaling proteins in single cells. Science 2000;287:1652–5.
[67] Duke TA, Le Novere N, Bray D. Conformational spread in a ring of proteins: a stochastic approach to allostery. J Mol Biol 2001;308:541–53.
[68] Bai F, Branch RW, Nicolau Jr DV, Pilizota T, Steel BC, Maini PK, et al. Conformational spread as a mechanism for cooperativity in the bacterial flagellar switch. Science 2010;327:685–9.
[69] Bai F, Minamino T, Wu Z, Namba K, Xing J. Coupling between switching regulation and torque generation in bacterial flagellar motor. Phys Rev Lett 2012;108:178105.
[70] Yuan J, Farner KA, Turner L, Berg HC. Asymmetry in the clockwise and counterclockwise rotation of the bacterial flagellar motor. Proc Natl Acad Sci U S A 2010;107:12846–9.
[71] Fahrner KA, Ryu WS, Biomechanics Berg HC. Bacterial flagellar switching under load. Nature 2003;423:938.
[72] Yuan J, Fahrner KA, Berg HC. Switching of the bacterial flagellar motor near zero load. J Mol Biol 2009;390:394–400.
[73] Wang F, Shi H, He R, Wang R, Zhang R, Yuan J. Non-equilibrium effect in the allosteric regulation of the bacterial flagellar switch. Nat Phys 2017;13:710–4.